nature energy

REVIEW ARTICLE

https://doi.org/10.1038/s41560-021-00973-9

Check for updates

Gas diffusion electrodes, reactor designs and key metrics of low-temperature CO_2 electrolysers

David Wakerley[1,2,9], Sarah Lamaison[1,2,3,9], Joshua Wicks[4,9], Auston Clemens[5,9], Jeremy Feaster[5,9], Daniel Corral[1,5,9], Shaffiq A. Jaffer[6], Amitava Sarkar[1,5,7], Marc Fontecave[3], Eric B. Duoss[5], Sarah Baker[5], Edward H. Sargent[4] ✉, Thomas F. Jaramillo[1,8] ✉ and Christopher Hahn[5,8] ✉

CO_2 emissions can be recycled via low-temperature CO_2 electrolysis to generate products such as carbon monoxide, ethanol, ethylene, acetic acid, formic acid and propanol. In recent years, progress has been made towards an industrially relevant performance by leveraging the development of gas diffusion electrodes (GDEs), which enhance the mass transport of reactant gases (for example, CO_2) to the active electrocatalyst. Innovations in GDE design have thus set new benchmarks for CO_2 conversion activity. In this Review, we discuss GDE-based CO_2 electrolysers, in terms of reactor designs, GDE composition and failure modes, to identify the key advances and remaining shortfalls of the technology. This is combined with an overview of the partial current densities, efficiencies and stabilities currently achieved and an outlook on how phenomena such as carbonate formation could influence the future direction of the field. Our aim is to capture insights that can accelerate the development of industrially relevant CO_2 electrolysers.

Anthropogenic CO_2 emission from the combustion of fossil fuels is projected to increase global temperatures by 1.5 °C between 2030 and 2052[1], which must be mitigated to protect Earth's existing biomes. Decreasing CO_2 emissions may, in part, be achieved through the continued introduction of renewable energy and electrification of the heating and transportation sectors, yet there remain key sectors that cannot easily be decarbonized. This is particularly true for air transportation, for which no electrified alternative is commercially available, or industries such as steel and cement, which require carbon oxidation in their operation. The carbon footprint of these sectors must instead be decreased through the implementation of renewable fuels and the conversion of CO_2 emissions, both of which may be addressed with CO_2 electrolysis.

A CO_2 electrolyser converts CO_2 into chemicals through the electrochemical reduction of its C–O bonds. Currently, electrolysers are split between two technologies: high-temperature (>600 °C) solid oxide electrolysers[2] and low-temperature (25–80 °C) electrolysers. CO_2 electrolysis to CO with solid oxide electrolysers has seen substantial progress at high temperatures, which is described elsewhere[2]. This review focuses on low-temperature electrolysers, a rapidly evolving field that continues to implement new reactor designs and catalyst types. Low-temperature CO_2 electrolysis is able to generate a diverse range of products, such as CO, ethylene, formic acid or ethanol, depending on the number of electrons transferred and the number of CO_2 molecules that are coupled together (Fig. 1a). Technoeconomic and life-cycle analyses have offered targets to achieve an economically compelling implementation of low-temperature CO_2 electrolysis, and suggest technological advances are necessary to compete with the cost of chemicals derived from fossil sources[3–5]. Nevertheless, continued innovation and investment in renewable power is beginning to lessen this gap, as is progress towards selective, stable and efficient CO_2 electrolysers.

Studies of low-temperature CO_2 electrolysis that used solubilized CO_2 in water as the reactant provided fundamental knowledge that served as the foundation of this field[6]. However, achieving high rates of reaction in these conditions is limited given the low concentration (33 mM) (ref. [7]) and slow diffusion of aqueous CO_2 (diffusion coefficient $t_{CO_2} = 0.00176$ mm^2 s^{-1} at 20 °C) (ref. [8]). This has motivated research into gas diffusion electrodes (GDEs), that use gaseous CO_2 as a substrate. A schematic of a GDE is presented in Fig. 1b, which illustrates how gaseous CO_2 is fed directly to an interface between the catalyst and electrolyte. This facilitates the rapid mass transport of CO_2 to the catalyst surface, where it is bound and subjected to the proton and electron transfers necessary to form a given product. Adoption of GDEs in the field of CO_2 reduction has provided new design concepts and operating principles for this research, and such vapour-fed reactors are now approaching performances, in some aspects, commensurate with the expectations for commercial technology, as covered in numerous contemporary reviews[9–11]. As of 2021, record ethylene- and carbon-monoxide-production partial current densities surpass 1 A cm^{-2} (refs. [12,13]), similar to that of commercial H_2O electrolysers. Still, most reported energy efficiencies and reactor stabilities are currently inadequate for commercialization and the low CO_2 single-pass conversion, carbon efficiency and product selectivity introduce downstream separation costs to the reaction.

This review presents the current status of and future outlook for low-temperature CO_2 electrolysers. We tie together advances in the configurations of low-temperature CO_2 electrolysis reactors,

[1]SUNCAT Center for Interface Science and Catalysis, Department of Chemical Engineering, Stanford University, Stanford, CA, USA. [2]Dioxycle SAS, Bordeaux, France. [3]Collège de France, Sorbonne Université, PSL University, Laboratoire de Chimie des Processus Biologiques, CNRS UMR 8229, Paris, France. [4]Department of Electrical and Computer Engineering, University of Toronto, Toronto, Ontario, Canada. [5]Lawrence Livermore National Laboratory, Livermore, CA, USA. [6]TotalEnergies American Services Inc., Hopkinton, MA, USA. [7]TotalEnergies EP Research & Technology USA, LLC, Houston, TX, USA. [8]SUNCAT Center for Interface Science and Catalysis, SLAC National Accelerator Laboratory, Menlo Park, CA, USA. [9]These authors contributed equally: David Wakerley, Sarah Lamaison, Joshua Wicks, Auston Clemens, Jeremy Feaster, Daniel Corral. ✉e-mail: ted.sargent@utoronto.ca; jaramillo@stanford.edu; hahn31@llnl.gov

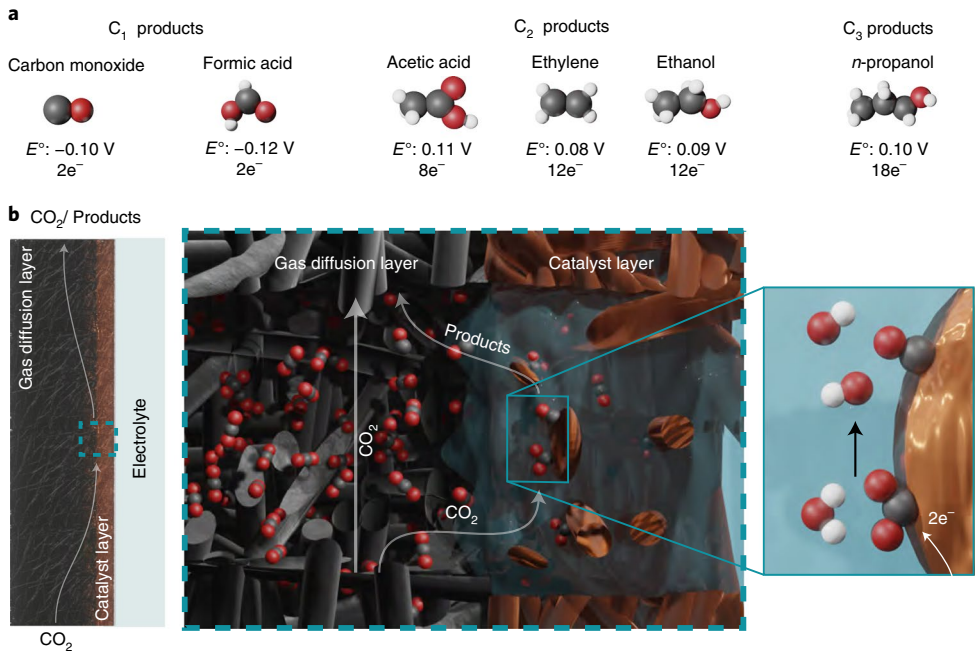

Fig. 1 | CO_2 electrolysis on a GDE. a, Common products of low-temperature CO_2 electrolysis, their thermodynamic redox potential against the RHE and the number of electron transfers necessary to form them. **b**, Schematic of a GDE in the operation of CO_2 electrolysis showing a section of the centre that illustrates the interface between the gas diffusion layer and catalyst layer. C, grey; O, red; H, white.

catalyst designs and failure modes with an analysis of the currently reported catalyst activity and stability. The ultimate goal is to establish the state of the field and highlight challenges that remain for the industrialization of this technology.

Component integration and reactor design

Component overview. The key components of the CO_2 electrolyser are presented in Fig. 2, which breaks down the structure of the gas diffusion layer, catalyst layer and membrane.

The gas diffusion layer is the gas-permeable support on which the catalyst layer is deposited (Figs. 1b and 2a). The layer controls the mass transfer of water, reactants and products to and from the catalyst layer and plays a role in determining the local environment around the catalyst. Most gas diffusion layers predominantly comprise a macroporous layer that permits diffusion of gaseous CO_2 from the reactant gas stream to the catalyst surface, as well as diffusion of gaseous products (for example, H_2, CO, CH_4 and C_2H_4) away from the catalyst surface to the gas stream. On top of the macroporous layer is often a microporous layer, which comprises carbon that has been treated with polymers, such as polytetrafluoroethylene (PTFE), to create a finely structured hydrophobic layer. Without the hydrophobic layer, electrolyte or water may flood the pores of the support (see the discussion in Failure modes and their solutions). Porous PTFE membranes are also viable gas diffusion layers[14] and contain a single layer: an insulating microporous sheet of hydrophobic PTFE fibres (Fig. 2b).

A catalyst layer is deposited on the gas diffusion layer, which provides the active sites on which CO_2 is bound and reduced. Catalyst designs include heterogeneous metals, molecular complexes and single-metal-atom-doped carbons. Heterogeneous metal catalysts comprise metal films, nanostructures and nanoparticles, the composition of which determines the products of CO_2 reduction: catalyst layers that comprise Ag (ref. [15]) and Au (ref. [16]) are predominantly used for CO production, Sn (ref. [17]) and Bi (ref. [18]) for formic acid production and Cu as a standalone catalyst[19,20] or in combination with other metals[21] for multicarbon products. Molecular catalysts are discrete transition metal complexes and include aromatic N-containing ligands (for example, porphyrins, phthalocyanines and/or bipyridine)[22]. Single-metal-atom-doped carbons use a metal ion bound within a carbonaceous host structure. These may be metal- and N-doped carbons (M–N–Cs), in which multiple nitrogen sites facilitate the ligation of a central single metal atom[23] or single atoms doped directly into graphitic carbon[24].

The anode in a CO_2 electrolyser is most commonly IrO_x (ref. [25]), Pt (ref. [26]), Ni (ref. [13]) or NiFe (refs. [27,28]) based. IrO_x nanoparticles on GDEs are used most consistently in high-energy-efficiency systems[16]. The anode carries out a complementary oxidation reaction to CO_2 reduction, which is most commonly water oxidation. Water oxidation in combination with CO_2 reduction is precisely the opposite of fossil fuel combustion, but its large voltage requirement (1.23 V versus the reversible hydrogen electrode (RHE)) has led to the consideration of alternative oxidation reactions, such as glucose to gluconic acid (−0.07 V versus RHE) or glycerol to glyceraldehyde (0.41 V versus RHE)[29].

Between the anode and cathode sits an ion-exchange membrane; a polymer sheet that transfers ions between the electrodes and hinders product crossover (Fig. 2c). These membranes are divided into three categories according to their ionic permeability: cation-exchange membranes (CEMs), anion-exchange membranes (AEMs) and bipolar membranes (BPMs)[30]. CEMs (for example, Nafion) conduct protons and/or cations via negatively charged functional groups, such as sulfonates, and AEMs (for example, Sustainion and PiperION) conduct anions via positively charged functional groups, such as imidazoliums or tertiary amines (Fig. 2d). BPMs combine an AEM and CEM around a central water dissociation (WD) layer that splits water into protons and hydroxide ions. Figure 2e shows the set-up of a BPM in which protons conduct from the BPM WD layer through the CEM and neutralize the hydroxide ions generated at the cathode, and WD-derived hydroxide ions cross the AEM to neutralize protons generated at the anode. This allows a distinct electrolyte pH to be maintained in each compartment and avoids concentration polarization losses[9]; however, the series resistance of the full electrochemical reactor using BPMs is normally higher than those of AEMs and CEMs[31]. Nevertheless,

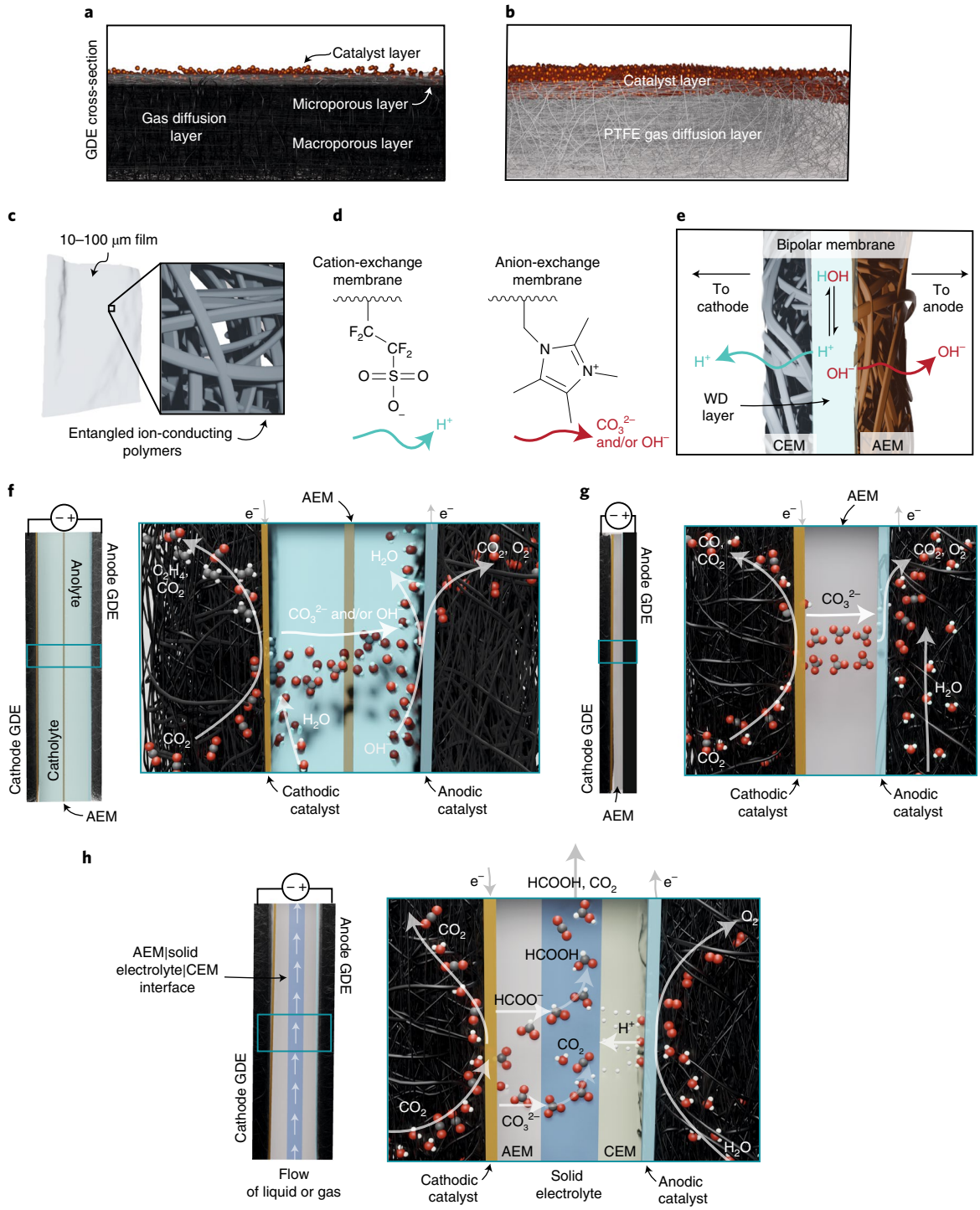

Fig. 2 | Components of a GDE CO_2 electrolyser. a,**b**, Gas diffusion layers used to fabricate GDEs, which display the catalyst layer added onto a conducting carbon paper (**a**) and a PTFE gas diffusion layer (**b**). **c**–**e**, A depiction of a typical membrane (**c**), functionalities from CEMs (left) and AEMs (right) (**d**) and their combination in a BPM that contained a WD layer (**e**). **f**, Schematic of an aqueous vapour-fed reactor for ethylene formation with an AEM. **g**, Schematic of a vapour-fed MEA for CO production with an AEM. **h**, Schematic of a vapour-fed SED for formic acid production with an AEM, central solid electrolyte and CEM. C, grey; O, red; H, white.

recent advances in BPMs have lowered the resistances across the cell, which greatly facilitates their use in electrocatalytic reactions[32].

Device operation and carbonate formation. GDE-driven CO_2 electrolysis is most selective and efficient when operating in locally neutral to basic pH conditions, because parasitic proton reduction to H_2 becomes favoured in locally acidic conditions. During the electrolyser operation in such conditions, CO_2 travels to the interface between the GDE and the catalyst layer, where it is reduced to a given product and OH^- is released, as shown in equation (1):

$$xCO_2 + (2x + y - z)H_2O + (4x + y - 2z)e^- \rightarrow C_xH_yO_z + (4x + y - 2z)OH^- \quad (1)$$

The hydroxide then reacts with inbound CO_2 to produce bicarbonate and carbonate anions through reactions (2) and (3):

$$CO_2 + OH^- \rightarrow HCO_3^- \quad (2)$$

$$HCO_3^- + OH^- \rightarrow CO_3^{2-} + H_2O \quad (3)$$

When using an AEM, OH^- is expected to carry charge from the cathode to the anode. However, it has been observed that in a CO_2 electrolyser, CO_3^{2-} may act as the charge carrier[12,33]. At the anode the charge carrier (CO_3^{2-} or OH^-) is oxidized to CO_2 and/or O_2 (equations (4) and (5) and the nature of the carrier may be quantified from the CO_2:O_2 ratio in the anodic outlet stream. As shown in reaction (5), a 2:1 ratio implies that CO_3^{2-} is the majority charge carrier and values lower than 2:1 of CO_2:O_2 imply that OH^- is, at least partially, undertaking the charge carrying role[34]:

$$2OH^- \rightarrow O_2 + 2H^+ + 4e^- \quad (4)$$

$$2CO_3^{2-} \rightarrow 2CO_2 + O_2 + 4e^- \quad (5)$$

Note that reaction (5) will not release CO_2 if the electrolyte is strongly basic, and therefore this diagnostic only works in 'steady-state' conditions, that is, when carbonate is converted at the anode at the same rate as it is produced at the cathode[35]. Recent discussion highlighted the energetic losses associated with using basic electrolytes that operate outside steady-state conditions, that is, when more CO_2 is consumed than released. A stable operation in such basic conditions requires constant removal of the carbonate from water, which requires >230 kJ mol^{-1} using an optimized calcination cycle[35], equivalent to >1.5 kWh kg^{-1} CO_2 removed. For comparison, a CO_2 electrolyser working at 2.3 V and 95% selectivity for CO production requires 2.9 kWh kg^{-1} CO_2 converted.

Reactor design. The above-mentioned components must be designed to facilitate reactions (1), (4) and (5) for an efficient CO_2 conversion. The transition from solubilized CO_2 reduction in 'H cells' was facilitated by the aqueous vapour-fed reactor (Fig. 2f)[36]. In this case, a cathode GDE sits at the interface of the inbound CO_2 and the flowing aqueous electrolyte (the catholyte), which is separated from the anodic electrolyte stream (the anolyte) by a central membrane. The electrolyte in the aqueous reactor contains alkali metal salts that ensure an adequate conductivity between the electrodes and is also able to improve the catalytic activity[25]. K^+ cations are typically used due to their availability, but Cs^+ was shown to improve multicarbon-product formation on planar Cu (ref. [37]) and to decrease the required potential for CO production[25,38]. The anion is typically hydroxide, but the consumption of CO_2 by hydroxide (equations (2) and (3) presents energetic losses that are not acceptable in large-scale CO_2 valorization[34,35,39]. Alternatively, halide anions were shown to suppress H_2 evolution and weaken the C–O bonds in surface-bound intermediates through an increased electron donation to the catalytic layer[40–42].

Membrane electrode assembly (MEA) electrolysers present higher efficiencies due to the lowered ohmic resistance of the zero-gap design. In a MEA electrolyser, the membrane is contacted on either side by the cathode and anode catalyst layers (Fig. 2g). During operation, the cathodic side is fed humidified CO_2 but no flowing electrolyte. The anode is typically fed an electrolyte of bicarbonate or carbonate and is commonly a porous Ti (ref. [43]) or a carbon gas diffusion layer[44] with deposited IrO_x nanoparticles. Introduction of both the anolyte and CO_2 uses a conducting plate with a flow field, which also provides an electrical contact to the MEA. A precise flow-field design is proving to be important for the development of the MEA reactor, with circular[12] or serpentine designs[45] both providing effective reactant transport.

The membrane in the MEA serves as both the electrolyte and product separator and has thus far been mostly based on AEMs. Sustainion membranes are based on a copolymer of imidazolium-functionalized styrene and styrene, and were used in MEAs that produce CO, formic acid and multicarbon products over record-breaking timescales[15,46–48]. Poly(aryl piperidinium) membranes (such as PiperION) have emerged as an alternative AEM that offers an increased basic stability over Sustainion thanks to an aromatic backbone; recently reported PiperION-based MEAs achieved a partial current density (j_{CO}) up to 1 A cm^{-2} (ref [12]), and a similar functionality was able to operate at 65% energy efficiency (EE) at 200 mA cm^{-2} for CO production[45]. The design of new AEMs is now paramount to further progress in this field, as recently reviewed[49].

To target the high-efficiency production of liquid products, solid electrolyte devices (SEDs) were developed. An example of such a reactor for formic acid production is presented in Fig. 2h; in this case, the reactor employs an AEM next to the cathode, a CEM next to the anode and a central solid electrolyte. The solid electrolyte may be a styrene–divinylbenzene sulfonated copolymer[18,50] or an ion exchange resin, such as Amberlite[51], which both protonates the product and allows its collection through a flowing liquid/gas carrier stream. Through this design, cells that contain a two-dimensional Bi cathode GDE and an IrO_x anode GDE have generated formic acid streams of 1.8 M at 200 mA cm^{-2} (FE formic acid, 80%) at a 2.7 V cell potential[50], and a similar system with a CuO cathode generated a solution of 4.6 mM ethanol, 3.4 mM *n*-propanol and 1.3 mM acetic acid at a cell voltage of 3.45 V at 94 mA cm^{-2} (j_{total}) (ref. [50]).

Each reactor presents different advantages that can be exploited for a given goal, for example, a high electrolyte adaptability in the

Box 1 | Calculating Faradaic efficiency and partial current density

Faradaic efficiency provides a measure of the selectivity of electron transfer from the electrode to the substrate. After quantifying the products of CO_2 reduction, the Faradaic efficiency may be calculated through equation (6):

$$FE_x(\%) = \frac{n_x \times n_{e^-x} \times F}{Q} \times 100 \quad (6)$$

Where n_x is the amount of product x (mol), n_{e-x} is the number of electrons to make x from CO_2/H_2O, F is the Faraday constant (96,485 C mol^{-1}) and Q is the total charge passed. As gaseous products are analysed within a stream of flowing CO_2, the CO_2 mass balance must be measured and calculated accurately to determine the FEs as CO_2 moves across the electrolyser according to reactions (2), (3) and (5).

After measuring the FE, analysis of the catalyst activity is provided through the partial current density. Despite cathodic currents generally being displayed as negative, partial current densities may be reported as absolute current values, as in equation (7):

$$j_x = \frac{|i|FE_x}{A} \quad (7)$$

where j_x is the partial current density for product x (mA cm^{-2}), i is the current passed by the electrode (mA) and A is the area of the electrode (cm^2). The partial current density is crucial as it relates selectivity to rate, which is essential when aiming to improve the technological viability of low temperature CO_2 reduction.

aqueous vapour-fed reactor, a low cell resistance in an MEA or liquid product collection in a SED. As CO_2 electrolysis continues to advance, the evolution of the reactor is proving paramount to stability, efficiency and operation at scale.

Catalyst integration in GDEs. The adoption of GDEs in low-temperature CO_2 electrolysis has introduced new means to integrate the CO_2-reducing catalyst. The ultimate properties of the CO_2 conversion reaction when using a GDE is dependent on the design of the catalyst, its integration with the gas diffusion layer and its surrounding microenvironment. The discussion of such factors in this section is supplemented by *j*–*E* curves, which show the rate of product formation (proportional to *j* (Box 1)) at a given efficiency (inversely proportional to the potential, *E*). Such curves are shown for CO, ethylene, ethanol and acetic acid production in Fig. 3. The potentials are converted into the standard hydrogen electrode (SHE) to facilitate their comparison on an absolute scale, and a catalytic onset versus SHE is defined based on the potential required to reach a j_x of 10 mA cm^{-2} for product *x*. This value represents a sufficiently high *j* to be unambiguously measured and compared between multiple reports, and avoids mass transport limitations and uncertainties in the electrode from *iR* correction, which is exacerbated at a high *j*.

Catalyst GDEs for CO production. The deposition of Ag nanoparticles onto gas diffusion layers with Nafion for binding has proved an effective route to selective CO production on GDEs (Fig. 3a)[52,53]. Alternative Ag morphologies, such as Ag corals[54], and the addition of catalyst supports, such as carbon foams[55] and multiwalled carbon nanotubes (MWCNTs)[56], proved effective at lowering the required Ag loading (Fig. 3a), but did not significantly change the activity. Instead, the reaction conditions have proved the most effective route to alter GDE activity: the lowest reported potential to reach a j_{CO} of 10 mA cm^{-2} on Ag is −1.04 V versus SHE and was achieved using nanoparticles with Cs^+-based electrolytes (blue pentagons in Fig. 3a) in optimized conditions (3 M CsOH electrolyte, 2.5 ml min^{-1} CO_2 flow rate, 1 bar CO_2 and a 2 mg cm^{-2} Ag nanoparticle loading). Electrochemical impedance spectroscopy showed a lowered charge transfer resistance at the catalytic interface when using Cs^+ cations, which implied that larger cations help stabilize the rate-determining M−CO_2^- intermediate[25].

Au nanoparticles were integrated onto GDEs through a preliminary deposition onto a support, such as carbon black[26,45] or multiwalled carbon nanotubes[16], or were deposited directly into the microporous layer[57]. This allows small nanoparticles (<10 nm) to be distributed over large electrochemical surface areas, yet even <0.2 mg cm^{-2} Au-containing GDEs still reach j_{CO} as high as 540 mA cm^{-2} (FE_{CO} 92%)[57]. Such Au-containing GDEs show the lowest onset potential for CO production of any heterogeneous metal surface at −0.96 V versus SHE (Fig. 3b).

Single-metal-site catalysts and molecular complexes implemented in GDEs exhibit a diverse range of onset potentials (Fig. 3c). At neutral pH, these materials can compete with Au: the lowest onset potential versus SHE was achieved using Fe^{3+} dispersed in pyrrolic-N sites, which showed a pH-dependent j_{CO} onset (green circles in Fig. 3c)[28]. The use of Ni single sites embedded in membranes (green squares in Fig. 3c), in MOFs[23] (downward green triangles) or as Ni–N–Cs[58,59] (blue circles and upward triangles, respectively) have also achieved low onset potentials, particularly in neutral pH (ref. [60]). The molecular catalysts Co phthalocyanine (blue triangles)[61] and Fe porphyrin (blue diamonds)[62] show similar onset potentials, but do not reach current densities as high, yet their potential to be modified make them particularly interesting for future study, as they have already shown promise in microfluidic and flow reactors[22].

Cu-based catalyst GDEs for C_2 production. Proposed steps in the production of ethylene, ethanol and acetic acid on Cu are presented in Fig. 4a, specifically highlighting instances in which a Cu-based catalyst integrated into a GDE has promoted and/or disfavoured certain intermediates towards a given product. The *j*–*E* curves for ethylene production on Cu-containing GDEs are shown in Fig. 3d.

Theoretical studies give evidence that Cu(100) surfaces facilitate ethylene production more effectively than Cu(111) and Cu(211) surfaces due to their increased activity for CO dimerization (Fig. 4a) and, when integrated into a GDE, Cu(100) functioned at the lowest reported overpotential for a pure Cu catalyst (dark blue squares in Fig. 3d) to achieve a $j_{ethylene}$ of 391 mA cm^{-2} ($FE_{ethylene}$ of 67% at −0.72 V versus RHE, 7 M KOH)[47]. At higher current densities, little difference is seen between the Cu(100) surface and catalysts based on Cu thin films (green circles)[63] or nanoporous morphologies of Cu (green pentagons)[19], which implies that other catalyst layer modifications are necessary to improve the intrinsic activity of Cu at a high rate.

At the time of writing, a fluorinated Cu catalyst integrated in a GDE displays the lowest reported ethylene production potential of −1.14 V versus SHE at a 10 mA cm^{-2} $j_{ethylene}$ (light blue diamonds in Fig. 3d), which is assigned to the enhanced dissociation of H_2O to form *CHO, key to ethylene formation, through the presence of surface fluoride (Fig. 4a)[27]. The integration of Cu-based alloys on GDEs is also able to increase ethylene selectivity due to the altered binding strength of key catalytic intermediates[64]. CuAg alloys show a superior activity to pure Cu (FE 60%, $j_{ethylene}$ 180 mA cm^{-2} (ref. [21])), which is assigned to the stabilization of active Cu_2O states in the presence of Ag. CuAl alloys have achieved a 75% $FE_{ethylene}$ at a $j_{ethylene}$ of 450 mA cm^{-2}, which is assigned to the ideal H* and CO* binding energy of CuAl sites for C_2 products, as predicted by density functional theory and machine learning[65]. Alternatively, ethylene-producing GDEs have benefitted from the combination of Cu with a CO-producing catalyst to increase the CO availability for C_2 production at lower overpotentials, called 'tandem catalysis'. Such a strategy was demonstrated through the addition of Ni–N–Cs on a Cu catalyst layer for ethylene generation[66] or of CO-producing Ag nanoparticles next to ethylene-producing Cu nanoparticles[67].

Cu-based GDEs also show a high affinity for ethanol production[68], and typically display a peak production rate of around −1.4 to −1.5 V versus SHE, as shown in Fig. 3e. The *j*–*E* dependence of each reported catalyst layer is similar, but the absolute selectivity towards ethanol ($FE_{ethanol}$) is dependent on the surface's disposition towards ethylene versus ethanol formation. As such, strategies to increase the selectivity for ethanol have centred around suppressing the surface propensity towards ethylene formation. To date, the most selective GDE for ethanol production achieved a $FE_{ethanol}$ of 52% ($j_{ethanol}$ 104.4 mA cm^{-2}) (light blue squares in Fig. 3e) using a layer of N-doped C on Cu to suppress the deoxygenation of surface HC−COH*, an ethylene-forming pathway, to instead encourage its protonation to ethanol-forming HC−CHOH* (Fig. 4a)[69]. Similarly, $Ce(OH)_x$ nanoparticles were used on Cu to promote the formation of surface-adsorbed H, which protonate HC−COH* (Fig. 4a) to encourage ethanol over ethylene formation (light blue plain circles in Fig. 3e)[70]. Nevertheless, despite the high selectivity, the onset potential for ethanol formation is not enhanced in these systems compared with those of other Cu-based GDEs (Fig. 3e).

Acetic acid is also commonly formed on Cu-based GDEs and is sensitive to electrode pH, as exemplified by the *j*–*E* curve in Fig. 3f. Acetic acid is believed to form through a ketene intermediate that irreversibly converts into acetic acid through a chemical reaction with OH^- (Fig. 4a)[71]. This chemical step can explain the potential-independent linear regions of the *j*–*E* curve seen in past studies[47,72,73] and visible in Fig. 3f. The reaction with this ketene intermediate has been exploited to form acetamides over acetic acid, opening the path for a broad range of chemical reactions to be explored[71]. Acetic acid is a more common product when using CO as the reactant in basic-pH electrolytes, with reported FEs up to

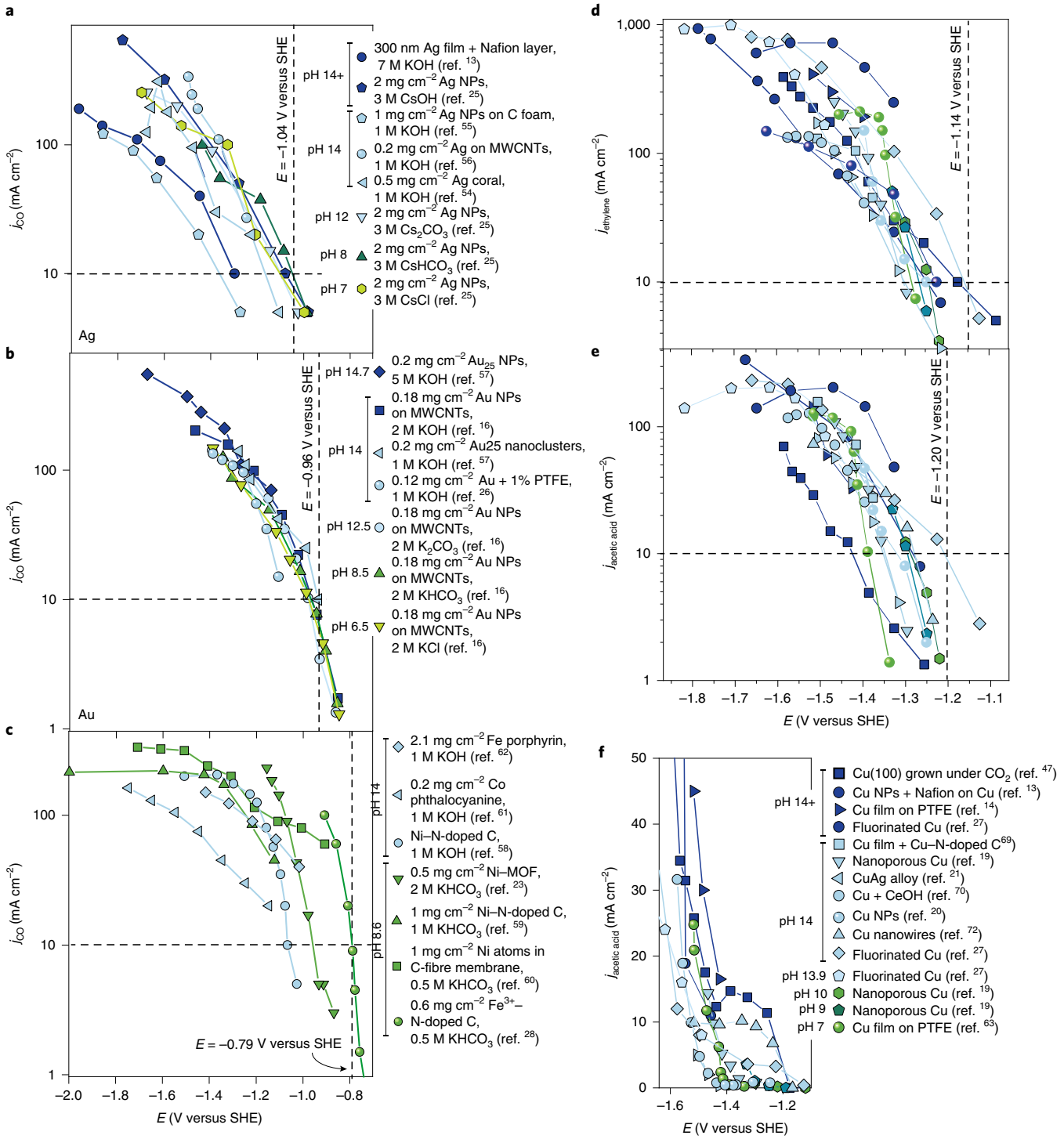

Fig. 3 | Benchmarks in potential-dependent activity. a–c, *j*–*E* analysis of contemporary reports for GDE-based CO_2-to-CO conversion on Ag (refs. [13,25,54–56]) (**a**), Au (refs. [16,26,57]) (**b**) and single-metal-atom or molecular catalysts[23,28,58–62] (**c**). **d–f**, *j*–*E* analysis of Cu-based GDEs for ethylene (**d**), ethanol (**e**) and acetic acid formation (**f**)[13,14,19–21,27,47,63,69,70,72]. The dashed lines indicate the lowest potential reported to achieve a current density of 10 mA cm^{-2}. Points are coloured based on the solution pH: light green, 6.5 < pH < 8; dark green, 8 < pH < 11; light blue, 12 < pH < 14; dark blue, pH > 14.

48% ($j_{\text{acetic acid}}$ of 131 mA cm^{-2}) (refs. [74,75]); this can be explained by a higher [OH$^-$] at the electrode interface during CO reduction due to the absence of carbonate formation.

Optimizing the catalyst microenvironment on a GDE. The microenvironment refers to the micrometre-scale three-dimensional space around the catalytic interface in which electronic and physical properties may be adapted to elicit changes in the catalyst properties. The three-dimensional structure of the GDE is particularly amenable to modification of the microenvironment, which allows GDE catalysis to be improved substantially beyond the possibilities afforded by a planar catalyst surface[39].

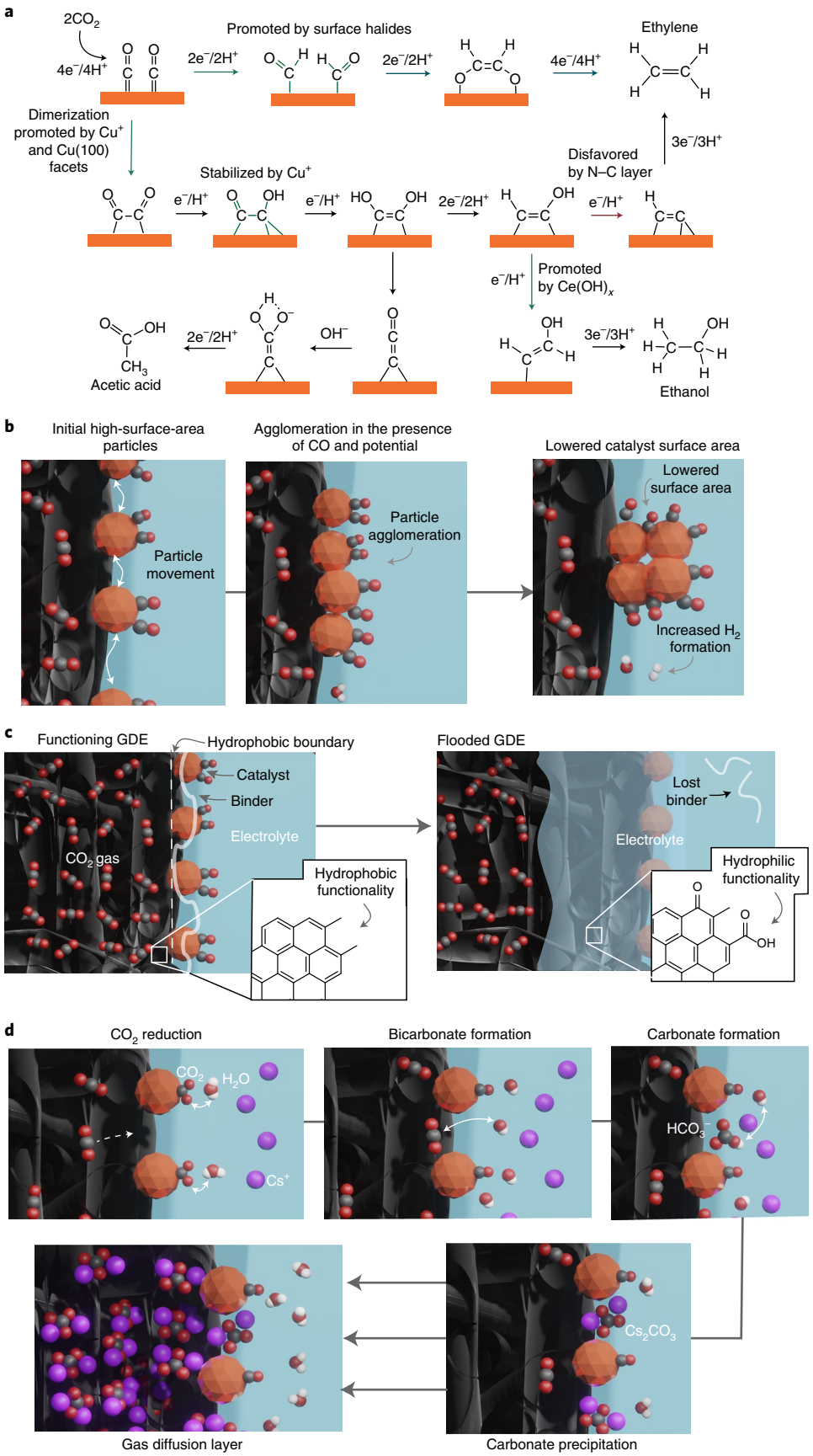

Fig. 4 | C_2 reaction pathways and common failure modes on GDE reactor cathodes. a, Pathways for C_2 product formation on Cu-based catalyst layers investigated on GDEs. **b**, Catalyst translation and agglomeration under a CO atmosphere during electrolysis. **c**, GDE flooding from the loss of hydrophobicity during operation. **d**, The formation of bicarbonate and carbonate ions from the reaction of CO_2 with OH^- followed by the formation and deposition of carbonate salt in the presence of Cs^+. C, grey; O, red; H, white; Cs, purple.

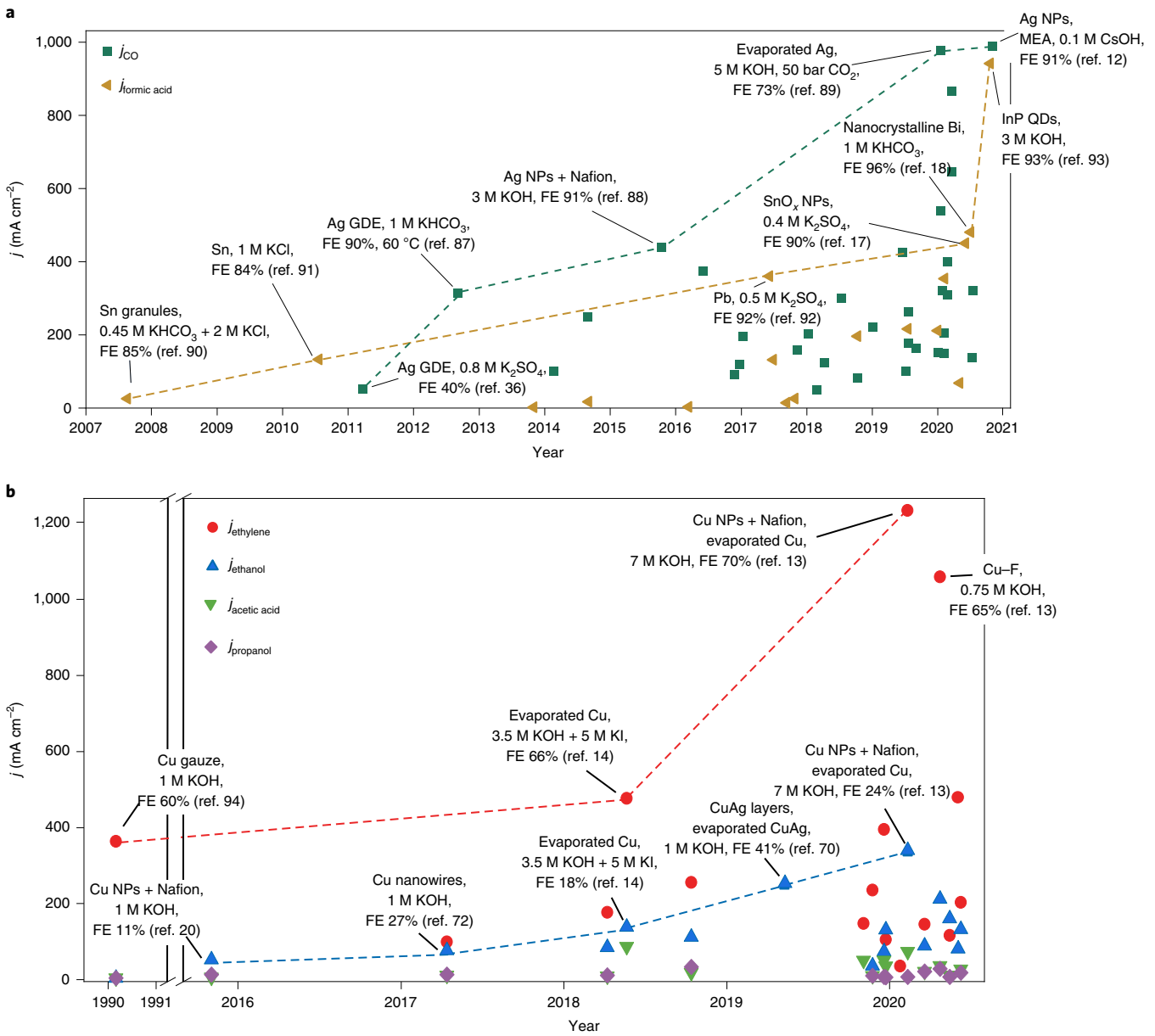

Fig. 5 | Metrics and progress in activity. a,**b**, Progress in partial current densities for various CO_2 reduction products, which include CO (refs. [12,36,87–89]) and formic acid[17,18,90–93] (**a**) and the multicarbon products ethylene[13,14,27,94], ethanol[13,14,20,70,72], acetic acid and propanol (**b**). The dashed lines show the activities in terms of current density over time. QD, quantum dots.

One common method to improve the GDE microenvironment for CO_2 electrolysis is to increase gas transport to the active catalyst. This may be achieved through the introduction of ionomers, ion conducting polymers that introduce both ionic functionality and hydrophobic organic structures. For example, the introduction of Nafion to a Ag film improved j_{CO} to a maximum of 400 mA cm^{-2}, compared with 50 mA cm^{-2} on a bare equivalent, due to increased mass transport of CO_2 and ionic species (dark blue circles in Fig. 3a)[13]. The same study describes the integration of Nafion ionomer with Cu NPs to increase CO_2 mass transport to the active sites, which results in a $j_{ethylene}$ of 930 mA cm^{-2} at 60% $FE_{ethylene}$ (dark blue circles in Fig. 3d)[13]. Improved gas transport has also been achieved through the combination of carbon black and 1% PTFE in the catalyst microenvironment to increase the local hydrophobicity. The resulting GDE is able to maintain an 80% CO_2 concentration at the triple-phase boundary at a high current density, and thereby decrease the potential CO_2 loss to the electrolyte[26].

Alternatively, the microenvironment may be adapted to improve its properties for catalytic intermediates. This was exemplified through the use of polydiallyldimethyl ammonium ionomers on Pd catalysts, which facilitated CO desorption from the catalytic surface. The resulting catalyst achieved a FE_{CO} of 93% at a j_{CO} of 279 mA cm^{-2} at a lower overpotential than that of bare Pd (ref. [76]). Similarly, the addition of organic arylpyridiniums to the microenvironment on a Cu GDE lowered the energy of the pathway towards ethylene formation by encouraging favourable binding modes of the CO* intermediate[48]. This modification showed a further improvement on the extended electropolymerization of the arylpyridiniums, to reach a FE of 72% for ethylene formation at $j_{ethylene} = 232$ mA cm^{-2}.

As GDE catalysts continue to be developed, it is essential that further understanding of the microenvironment is prioritized, as

this will be key to reduce the catalytic potentials shown in Fig. 3, as well as avoid the use of highly alkaline environments[39]. Such developments may take inspiration from naturally occurring carbonate monoxide dehydrogenase enzymes, which are able to generate CO at the thermodynamic potential thanks to the ideal catalytic environment it presents[77].

Failure modes and their solutions

Catalyst failure. Catalyst failure refers to a chemical or physical change of the active catalyst sites that lowers the selectivity or rate of CO_2 reduction[78]. One of the most reported mechanisms of this failure on GDEs is through surface restructuration and/or leaching of the active catalyst. This is most observed with Cu-based catalysts, as Cu 3*d* valence orbitals form strong bonds with C- and O-based surface intermediates[79]. Cu particles may move and reconstruct on the GDE surface during electrolysis, as recently illustrated on a porous Cu shell–Ag core nanoparticle through operando transmission electron microscopy. Importantly this decomposition occurs below the potentials at which Cu reduces CO_2, so long as CO is present, which confirms a major role of CO in the destabilization of the catalyst[80]. This process both lowers the available catalyst surface area and exposes the gas diffusion layer underneath, both of which negatively impact the catalytic partial current densities and/or FEs for CO_2 reduction in favour of H_2 evolution (Fig. 4b). This reconstruction was also seen through the enrichment of Ag at the surface of a $Ag_2Cu_2O_3$ alloy GDE during operation, which led to a $0.1\%\,h^{-1}$ decrease in $FE_{ethylene}$ in favour of the concomitant increase in CO production[81].

Transition metal impurities are often present in ppm levels in electrolyte salts, which may also contaminate and deactivate a GDE. Deposition of these salts onto the catalyst layer surface during electrolysis increases the parasitic formation of H_2, particularly in reactors with high electrolyte concentrations[38]. Catalyst surface poisoning has been prevented using chelating agents, such as ethylenediaminetetraacetic acid (EDTA)[82] or solid-supported iminodiacetate resins (Chelex 100)[83], which remove metal impurities to stabilize long-term activity. Contamination of the catalyst surface may also occur through the deposition of carbonate, which is discussed below.

Cathode flooding. Owing to the requirement for both gas-phase CO_2 and H_2O in the CO_2 electrolyser, it is common for gas-diffusion-layer failure to occur through flooding, that is, failure as water penetrates the GDE and thereby hampers CO_2 transport to the catalyst (Fig. 4c)[84]. Flooding may occur after decomposition of the hydrophobic chemical structure of the gas diffusion layer, which is susceptible to the basic environment generated during cathodic CO_2 reduction. Decomposition mechanisms include oxidation of the graphitic functionality present in the sp^2 carbon of the support to hydrophilic acid, hydroxyl and/or carbonyl groups (Fig. 4c)[85]. A similar effect occurs when hydrophobic ionomers and/or PTFE binders in the catalyst layer break down[78]. Flooding may also occur from the movement of water that accompanies cation migration to the cathode GDE, which is prevalent at high voltages and elevated electrolyte concentrations.

Mitigation of flooding is manageable provided the cause is elucidated: rapid flooding may be a result of pressure imbalance[16], which can be accounted for with a change in CO_2 or electrolyte flow rate. However, flooding related to the more gradual loss of hydrophobicity may be placated through the use of less-basic electrolytes or the addition of hydrophobic surface additives, such as polymers with intrinsic microporosity[60] or carbonaceous species[14].

Carbonate salt formation. A failure mode unique to the CO_2 electrolyser is the contamination of the GDE by carbonate salts. Although carbonate salts are soluble in aqueous media, a high local concentration of carbonate due the reaction of CO_2 with hydroxide (reaction (2)) generated during electrolysis, combined with a cross over of cationic species, such as K^+, Na^+ and/or Cs^+ from the anolyte, causes carbonate salts to precipitate throughout the GDE, which hinders CO_2 diffusion pathways through the gas diffusion layer and thus decreases CO_2 activity (Fig. 4d)[86].

Carbonate salt formation is reversible, and reports describe that water may be flushed through the gas diffusion layer to dissolve excess carbonate[16]; however, other more-convenient methods are emerging to mitigate carbonate formation. For example, in a MEA that contains PiperION membranes for CO production, pure water could be used as the electrolyte, and so avoid the build-up of carbonate completely, provided that periodic MEA flushing with CsOH–isopropyl alcohol mixtures occurred every 12 hours. The flushing distributed Cs^+ throughout the cathode, which facilitated an efficient CO_2 reduction, and the resultant MEA operated for 210 hours at a j_{CO} of $350\,mA\,cm^{-2}$. Alternatively, the periodic switching to a low current density (near to $0\,mA\,cm^{-2}$) allows excess carbonate to migrate to the anode before it reaches a critical point of accumulation in a MEA. A system that incorporates this approach with

Box 2 | Energy efficiency and carbon efficiency

The EE of a system is commonly calculated through equation (8), otherwise known as the voltage efficiency:

$$EE_x(\%) = \frac{E_{thermo}}{E_{cell}} \times FE_x \tag{8}$$

where E_{thermo} is the thermodynamic potential of the electrolysis reaction to generate product x from CO_2 and E_{cell} is the potential applied across the reactor. This equation provides a measure of the voltage used to undertake the desired reaction versus the extra voltage necessary to overcome catalytic overpotentials, resistances, generation of side products and pH gradients.

The carbon efficiency, or single-pass conversion, establishes how much carbon that enters an electrolyser is converted into products versus the quantity unconverted or lost as a charge carrier (equation (9)):

$$\text{Carbon efficiency}\,(\%) = \frac{\sum C_x n_x}{n_{CO_2}} \times 100 \tag{9}$$

where C_x is the number of carbons in product x, n_x is the number of moles of product x created and n_{CO_2} is the number of moles of CO_2 that entered the system.

When carbonate is the sole charge carrier to cross the central membrane, a portion of the CO_2 stream is no longer available for conversion and the maximum possible carbon efficiency for a given product x drops to 50% or below, as shown in equation (10), simplified to equation (11):

$$\text{Maximum carbon efficiency for a product, } x\,(\%) = \frac{n_x C_x}{n_x C_x + n_{CO_3^{2-}}} \times 100 \tag{10}$$

$$\text{Maximum carbon efficiency for a product, } x\,(\%) = \frac{1}{1 + \frac{n_{e^-x}}{2C_x}} \times 100 \tag{11}$$

where $n_{CO_3^{2-}}$ is the amount of carbonate produced (equivalent to $n_x n_{e^-x}/2$) and n_{e^-x} is the number of electrons needed to make n_x.

a Cu nanoparticle catalyst was able to function for 236 hours (157 hours of electrolysis and 79 hours of regeneration) at 175 mA cm^{-2} and 80% FE_{C2} (ref. [86]).

Progress and future perspective

Partial current density and selectivity. Figure 5a,b shows the current progress in *j* for CO, formic acid, ethylene, ethanol, acetic acid and propanol formation, with high activities for the first four. Progress in the field over the past decade is immense and understanding the underlying advances is key for further improvements of this technology.

Systems with the highest j_{CO} values invariably use Ag (Fig. 5a) as it benefits from a high intrinsic activity (FE_{CO} typically >90%) and a low cost compared with those of Au (refs. [87,88]). Over the past ten years, the higher peak j_{CO} values from Ag nanoparticles have increased an order of magnitude, which results from the introduction of GDEs and catalyst-layer engineering. A j_{CO} that approaches 1 A cm^{-2} (FE_{CO} 73%) was initially achieved through the use of high pressures (50 bar CO_2) in alkaline solutions[89], but now progress in MEA design has led to a j_{CO} of 1 A cm^{-2} (90% FE_{CO}) at 1 bar CO_2 and 65 °C in 0.1 M CsOH electrolyte[12].

A substantial improvement in *j* and FE for formic acid production was similarly witnessed over the past 14 years (Fig. 5a). Sn was the first formic-acid-producing metal to be used in a GDE[90,91] and later Pb showed promising $j_{formic\ acid}$ values of up to 360 mA cm^{-2} ($FE_{formate}$ 92%)[92]. A higher $j_{formic\ acid}$ was achieved through the improvement in reactor design: a $j_{formic\ acid}$ of 450 mA cm^{-2} ($FE_{formic\ acid}$ 97%) was achieved using a nanocrystalline Bi catalyst in a SED, which encourages formic acid generation through an effective product collection[18]. Alternatively, aqueous reactors that contain BPMs can also effectively separate the cathodic and anodic chambers, and were recently exploited with a Sn-based catalyst layer to generate formic acid at 90% FE and a corresponding $j_{formic\ acid}$ of 450 mA cm^{-2} on a 25 cm^2 GDE[17]. A high formic acid production has recently been achieved on a GDE loaded with InP quantum dots, which are aided in catalysis by sulfur-containing capping ligands to attain a $j_{formic\ acid}$ of 930 mA cm^{-2} ($FE_{formic\ acid}$ 93%)[93].

The production of ethylene has been improved through the refinement of the Cu morphology and GDE design, as discussed above and in Fig. 3[94], which allows ethylene partial current densities to surpass 1 A cm^{-2} (refs. [13,27]). Ethanol has followed a similar trajectory to reach a $j_{ethanol}$ of 337 mA cm^{-2} at 24% $FE_{ethanol}$ when using Cu nanoparticles in the presence of a Nafion binder[13]. The green triangles and purple diamonds in Fig. 5b show that the production of acetic acid and *n*-propanol, respectively, have not witnessed the same improvements and continue to be produced with a low selectivity. Acetic acid values sit below 100 mA cm^{-2} and $j_{propanol}$ at around 30 mA cm^{-2}. Selectivity for both products is superior in a highly basic pH, which may suggest both are dependent on chemical reactions with hydroxide that are not potential dependent[95–97].

When envisioning the technological roll out of low-temperature CO_2 electrolysis, partial current densities from reactors at smaller scales can aid in assessing the capital expenditure of the device at larger scales, that is, the size of the electrolytic reactor necessary to reach a given rate of CO_2 conversion. The achieved current densities for CO, ethylene and formic acid now surpass the values designated by techno-economic analysis as potentially profitable[3,4]. However, these models suggest that energy efficiencies (Box 2) must be improved as the operational costs (energy consumption) are sensitive to this parameter. For this reason, future developments must focus on lowering the potential at which a given partial current density is achieved. As discussed in the following sections, this will require further research into the characterization and optimization of the GDE microenvironment to improve CO_2 mass transport and lower the catalytic barrier of key reaction intermediates.

Attention must also turn to the scale at which electrolysis is carried out. Typically, partial current densities are reported on electrodes <5 cm^2 to expediate the preparation and testing; however, this ignores complications unique to larger scales, such as heating associated with large amperages and the effective introduction of high volumes of CO_2. Mitigation of these issues will allow further industrial operation to be considered, such as variable power sources and low-purity CO_2, to facilitate the production of optimized CO_2 electrolysers on a mass scale. Fortunately, the few reports of large-scale electrolysis stacks have presented promising activity[43,98,99].

Reactor lifetime. Considerable progress has been made in increasing the CO_2 electrolyser durability for both the current density and EE for a given product, as can be seen in the GDE stability studies presented in Fig. 6a,b. This chart shows the lowest *j* (Fig. 6a) and EE (Fig. 6b) reported over the course of a stability test versus the duration of the test. If reported, the failure mode of the catalyst is highlighted by the shape of the symbol. A range of catalysts, such as Cu, Ag and Sn nanoparticles, thin films of Cu and Ni–N–Cs, have now endured >100 hours of electrolysis without failure, which suggest that the key to durability lies with the reactor and GDE design, rather than with the catalyst itself. The factor consistent with the high durability is the use of MEAs, which have reached >1,000 hours of continuous operation[15]. Commercially available Sustainion MEAs have now illustrated at least 3,800 hours of activity at 190 mA cm^{-2} (FE_{CO} 95%) with a Ag nanoparticle cathode and IrO_x anode[100], whereas in similar conditions PiperION has shown 210 hours at a j_{CO} of 350–410 mA cm^{-2} (ref. [98]).

Future investigation into electrolyser stability must focus on improving the reactor lifetime at higher rates, that is, >1,000 hours at partial current densities above 200 mA cm^{-2}. In such conditions, the likelihood of failure is exacerbated, which requires an in-depth understanding of a reactor's failure modes to ensure that adequate countermeasures can be introduced. Owing to the time-consuming nature of such exploration, it is in the interest of the field to develop accelerated ageing techniques to simulate a month of continuous electrolysis in a few hours[101]. This may be achieved by operating at higher temperatures, using higher molarity electrolyte or cycling between high and low current densities to accelerate the morphological changes of the catalyst surface[102]. The performance hysteresis from the latter may give insight into electrode durability under variable operations and turn-on and/or shut-down procedures of industrially implemented reactors.

EE and carbon efficiency. As mentioned above, EE will determine the operating cost of CO_2 electrolysis by determining the energy requirements of conversion. Figure 6b shows that the EE during low-temperature CO_2 electrolysis efficiency is typically 40% or lower over long-term experiments; CO production stabilizes at 40%

Fig. 6 | Durability of reported CO_2 electrolysers and the lowest achievable overpotentials. a,**b**, Reported stability of GDEs for CO (refs. [12,15,16,23,26,38,43,54,58,60–62,87,89,98–100,106,107]), formic acid (refs. [17,18,51,90,92,106,108–110]), ethylene (refs. [13,14,20,47,48,63,86] and ethanol (refs. [20,63,64,69,70]), which indicate the lowest (**a**) partial current density and EE (**b**) reported during electrolysis versus the time at which electrolysis was halted. The data point shapes indicate the primary mode of failure when reported. **c**, The change in thermodynamic potentials of key CO_2 electrolysis reactions with pH against the CO_2 reduction onset for CO, ethylene, ethanol and acetic acid reported on GDEs. The data points and the horizontal dashed lines represent the potential value against SHE required to reach 10 mA cm^{-2} of the curves in Fig. 3a–f for each product and the dashed vertical line indicates the overpotential (η) required to reach 10 mA cm^{-2} at pH 11.5 (the pH of a solution of 0.5 M K_2CO_3).

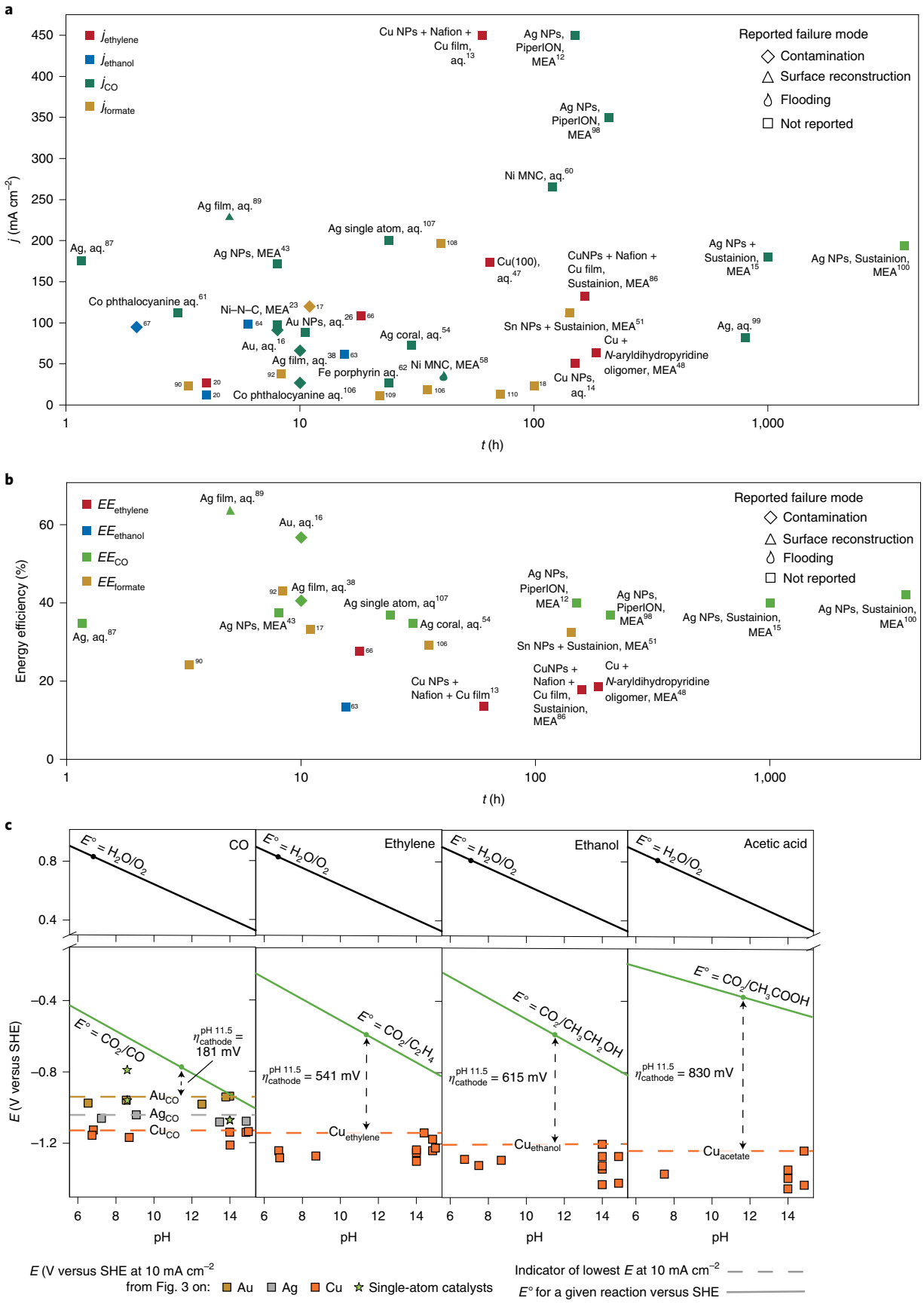
a
$j_{ethylene}$
$j_{ethanol}$
j_{CO}
$j_{formate}$
Reported failure mode
Contamination
Surface reconstruction
Flooding
Not reported
j (mA cm−2)
t (h)
Cu NPs + Nafion + Cu film, aq.13
Ag NPs, PiperION, MEA12
Ag NPs, PiperION, MEA98
Ni MNC, aq.60
Ag film, aq.89
Ag single atom, aq.107
Ag, aq.87
Ag NPs, MEA43
Cu(100), aq.47
CuNPs + Nafion + Cu film, Sustainion, MEA86
Ag NPs + Sustainion, MEA15
Ag NPs, Sustainion, MEA100
Co phthalocyanine aq.61
Ni–N–C, MEA23
Au NPs, aq.26
Sn NPs + Sustainion, MEA51
Ag, aq.99
Au, aq.16
Ag coral, aq.54
Cu + N-aryldihydropyridine oligomer, MEA48
Ag film, aq.38
Fe porphyrin aq.62
Ni MNC, MEA58
Cu NPs, aq.14
Co phthalocyanine aq.106
b
$EE_{ethylene}$
$EE_{ethanol}$
EE_{CO}
$EE_{formate}$
Reported failure mode
Contamination
Surface reconstruction
Flooding
Not reported
Energy efficiency (%)
t (h)
Ag film, aq.89
Au, aq.16
Ag film, aq.38
Ag single atom, aq107
Ag NPs, MEA43
Ag coral, aq.54
Ag, aq.87
Ag NPs, PiperION, MEA12
Ag NPs, PiperION, MEA98
Ag NPs, Sustainion, MEA15
Ag NPs, Sustainion, MEA100
Sn NPs + Sustainion, MEA51
Cu NPs + Nafion + Cu film13
CuNPs + Nafion + Cu film, Sustainion, MEA86
Cu + N-aryldihydropyridine oligomer, MEA48
c
CO
Ethylene
Ethanol
Acetic acid
$E° = H_2O/O_2$
$E° = CO_2/CO$
$E° = CO_2/C_2H_4$
$E° = CO_2/CH_3CH_2OH$
$E° = CO_2/CH_3COOH$
$\eta_{cathode}^{pH\ 11.5}$ = 181 mV
$\eta_{cathode}^{pH\ 11.5}$ = 541 mV
$\eta_{cathode}^{pH\ 11.5}$ = 615 mV
$\eta_{cathode}^{pH\ 11.5}$ = 830 mV
Au_{CO}
Ag_{CO}
Cu_{CO}
$Cu_{ethylene}$
$Cu_{ethanol}$
$Cu_{acetate}$
E (V versus SHE)
pH
E (V versus SHE at 10 mA cm−2 from Fig. 3 on: Au Ag Cu Single-atom catalysts
Indicator of lowest E at 10 mA cm−2
E° for a given reaction versus SHE

over 1,000 hours at 200 mA cm^{-2} (ref. [15]), formic acid production reaches 33% over 142 hours at 140 mA cm^{-2} (ref. [51]) and ethylene production MEAs have achieved 18% EE for ethylene production at 138 mA cm^{-2} over 157 hours (ref. [86]). This currently presents a major hurdle in the wide-scale adoption of this technology.

The low efficiency stems from the steady-state conditions imposed by carbonate formation (as discussed above). Ag, Au or Cu have absolute potentials (versus SHE) at which a given metal makes a given product, as illustrated by the horizontal dashed lines in Fig. 6c, which display the potentials required to reach 10 mA cm^{-2} for different products above pH 6. The pH-dependent thermodynamic potentials are illustrated by the solid black and green lines for the water oxidation and CO_2 reduction reaction, respectively. It can be seen that a GDE may achieve much lower cell potentials and resulting higher EEs at a high pH, as noted in several reports[16,38,103]. However, the reaction between CO_2 and hydroxide leads the local pH of the cathode to equilibrate around pH 11.5 (estimated based on the value of a 0.5 M K_2CO_3 solution) over continued operation[34]. The dashed vertical arrows in Fig. 6c indicate the cathode overpotential on different catalysts at pH 11.5, which adds a minimum of 181 mV to the overpotential for CO production (based on the overpotential achievable on Au catalysts). Multicarbon product overpotentials suffer considerably worse, at 541 mV for ethylene, 615 mV for ethanol and 830 mV for acetic acid.

The anodic overpotential is similarly compromised during steady-state operation as the release of CO_2 at the anode leads to a buffered pH of 7–8 (refs. [34,35]). Oxidation catalysts do not function efficiently in neutral conditions and anodic overpotentials of 800 mV were estimated to reach a current density of 200 mA cm^{-2} (ref. [35]).

Carbonate formation and cross over also hamper the reactor's carbon efficiency; the amount of carbon converted per pass through the electrolyser (Box 2). The release of CO_2 with O_2 at the anode introduces contaminated anodic streams, particularly with highly reduced products; for CO production, the maximum conversion of CO_2 through the cathodic stream is 50%, whereas for ethylene only 25% of the CO_2 in the gas stream can be converted in a single pass. To improve the carbon efficiency, the anode stream must be separated from the produced O_2 and reinjected into the cathodic stream, which introduces further energetic costs to the reactor.

The energetic downfalls associated with carbonate formation stand as a key hurdle in the adoption of low-temperature CO_2 electrolysis. Reconsideration of how carbonate formation may be managed, mitigated or avoided is crucial to determine the viability of the technology in the next few years of development. Many research pathways present solutions to this problem, which include the use of bulk acidic conditions[104], engineering of the ion exchange membranes[105] and fine-tuning of the catalytic microenvironment[39], yet time is needed to appreciate the efficacy of such strategies.

Conclusions

The collated data from the existing systems presented provide insights into how selectivity, efficiency and stability have been optimized to give a considerable improvement in low-temperature CO_2 electrolysers. The rapid progress in this field has inspired a shift from fundamentally to industrially inclined research, which now seeks to overcome the remaining hurdles before commercial roll-out, as is evident from corporate interest, the emergence of start-up companies and teams in the Carbon XPrize competition.

Presently, three key hurdles must be overcome to match the energy efficiencies of 70–80% possible in low-temperature H_2O electrolysis: The overpotentials for catalysis at a high current density must be reduced, particularly for multicarbon products, the reactor stability at a high current density must be improved and energy losses associated with carbonate formation must be mitigated. Whether or not this is possible will be determined by the advances made over the following years; however, at the fundamental level low-temperature CO_2 electrolysis remains one of the most elegant solutions to mitigate industrial CO_2 emissions.

Received: 22 January 2021; Accepted: 9 December 2021;
Published online: 17 February 2022

References

1. IPCC *Special Report Global Warming of 1.5 °C* (eds. Masson-Delmotte, V. et al.) Ch. 1 (WMO, 2018).
2. Hauch, A. et al. Recent advances in solid oxide cell technology for electrolysis. *Science* **370**, eaba6118 (2020).
3. De Luna, P. et al. What would it take for renewably powered electrosynthesis to displace petrochemical processes? *Science* **364**, eaav3506 (2019).
4. Jouny, M., Luc, W. & Jiao, F. General techno-economic analysis of CO_2 electrolysis systems. *Ind. Eng. Chem. Res.* **57**, 2165–2177 (2018).
5. Verma, S. et al. A gross-margin model for defining technoeconomic benchmarks in the electroreduction of CO_2. *ChemSusChem* **9**, 1972–1979 (2016).
6. Hori, Y. in *Modern Aspects of Electrochemistry* (eds Vayenas, C. G., White, R. E. & Gamboa-Aldeco, M. E.) 89–189 (Springer, 2008).
7. Sander, R. Compilation of Henry's law constants, version 3.99. *Atmos. Chem. Phys. Discuss.* **14**, 29615–30521 (2014).
8. Tamimi, A., Rinker, E. B. & Sandall, O. C. Diffusion coefficients for hydrogen sulfide, carbon dioxide, and nitrous oxide in water over the temperature range 293–368 K. *J. Chem. Eng. Data* **39**, 330–332 (1994).
9. Liu, K., Smith, W. A. & Burdyny, T. Introductory guide to assembling and operating gas diffusion electrodes for electrochemical CO_2 reduction. *ACS Energy Lett.* **4**, 639–643 (2019).
10. Burdyny, T. & Smith, W. A. CO_2 reduction on gas-diffusion electrodes and why catalytic performance must be assessed at commercially-relevant conditions. *Energy Environ. Sci.* **12**, 1442–1453 (2019).
11. Higgins, D., Hahn, C., Xiang, C., Jaramillo, T. F. & Weber, A. Z. Gas-diffusion electrodes for carbon dioxide reduction: a new paradigm. *ACS Energy Lett.* **4**, 317–324 (2019).
12. Endrődi, B. et al. High carbonate ion conductance of a robust PiperION membrane allows industrial current density and conversion in a zero-gap carbon dioxide electrolyzer cell. *Energy Environ. Sci.* **13**, 4098–4105 (2020). **The use of a PiperION membrane in a MEA reactor achieved current densities of > 1 A cm^{-2} for CO production from CO_2.**
13. García de Arquer, F. P. et al. CO_2 electrolysis to multicarbon products at activities greater than 1 A cm^{-2}. *Science* **367**, 661–666 (2020). **The combination of ionomer and catalyst particles to increase the diffusion of CO_2 to the active catalyst surface, achieving a peak current density for ethylene production of 1.3 A cm^{-2}.**
14. Dinh, C.-T. et al. CO_2 electroreduction to ethylene via hydroxide-mediated copper catalysis at an abrupt interface. *Science* **360**, 783–787 (2018).
15. Kutz, R. B. et al. Sustainion imidazolium-functionalized polymers for carbon dioxide electrolysis. *Energy Technol.* **5**, 929–936 (2017). **A report detailing the synthesis of Sustainion membranes and their use in MEA reactors achieving six months of continuous operation.**
16. Verma, S. et al. Insights into the low overpotential electroreduction of CO_2 to CO on a supported gold catalyst in an alkaline flow electrolyzer. *ACS Energy Lett.* **3**, 193–198 (2018).
17. Chen, Y. et al. A robust, scalable platform for the electrochemical conversion of CO_2 to formate: identifying pathways to higher energy efficiencies. *ACS Energy Lett.* **5**, 1825–1833 (2020). **A reactor design containing a bipolar membrane and flowing catholyte for the production of formic acid that could achieve 500 mA cm^{-2} on a 25 cm^2 gas diffusion electrode.**
18. Fan, L., Xia, C., Zhu, P., Lu, Y. & Wang, H. Electrochemical CO_2 reduction to high-concentration pure formic acid solutions in an all-solid-state reactor. *Nat. Commun.* **11**, 3633 (2020).
19. Lv, J.-J. et al. A highly porous copper electrocatalyst for carbon dioxide reduction. *Adv. Mater.* **30**, 1803111 (2018).
20. Ma, S. et al. One-step electrosynthesis of ethylene and ethanol from CO_2 in an alkaline electrolyzer. *J. Power Sources* **301**, 219–228 (2016).
21. Hoang, T. T. H. et al. Nanoporous copper–silver alloys by additive-controlled electrodeposition for the selective electroreduction of CO_2 to ethylene and ethanol. *J. Am. Chem. Soc.* **140**, 5791–5797 (2018).
22. Ren, S. et al. Molecular electrocatalysts can mediate fast, selective CO_2 reduction in a flow cell. *Science* **365**, 367–369 (2019).
23. Guo, J.-H., Zhang, X.-Y., Dao, X.-Y. & Sun, W.-Y. Nanoporous metal–organic framework-based ellipsoidal nanoparticles for the catalytic electroreduction of CO_2. *ACS Appl. Nano Mater.* **3**, 2625–2635 (2020).
24. Jiang, K. et al. Transition-metal single atoms in a graphene shell as active centers for highly efficient artificial photosynthesis. *Chem* **3**, 950–960 (2017).

25. Bhargava, S. S. et al. System design rules for intensifying the electrochemical reduction of CO_2 to CO on Ag nanoparticles. *ChemElectroChem* **7**, 2001–2011 (2020).
An in-depth study of Ag nanoparticle cathodes and their operating conditions for CO production, achieving a partial current density of 866 mA cm^{-2} at 43% energy efficiency.
26. Shi, R. et al. Efficient wettability-controlled electroreduction of CO_2 to CO at Au/C interfaces. *Nat. Commun.* **11**, 3028 (2020).
27. Ma, W. et al. Electrocatalytic reduction of CO_2 to ethylene and ethanol through hydrogen-assisted C–C coupling over fluorine-modified copper. *Nat. Catal.* **3**, 478–487 (2020).
28. Gu, J., Hsu, C.-S., Bai, L., Chen, H. M. & Hu, X. Atomically dispersed Fe^{3+} sites catalyze efficient CO_2 electroreduction to CO. *Science* **364**, 1091–1094 (2019).
29. Verma, S., Lu, S. & Kenis, P. J. A. Co-electrolysis of CO_2 and glycerol as a pathway to carbon chemicals with improved technoeconomics due to low electricity consumption. *Nat. Energy* **4**, 466–474 (2019).
30. Oener, S. Z., Ardo, S. & Boettcher, S. W. Ionic processes in water electrolysis: the role of ion-selective membranes. *ACS Energy Lett.* **2**, 2625–2634 (2017).
31. Pătru, A., Binninger, T., Pribyl, B. & Schmidt, T. J. Design principles of bipolar electrochemical co-electrolysis cells for efficient reduction of carbon dioxide from gas phase at low temperature. *J. Electrochem. Soc.* **166**, F34–F43 (2019).
32. Oener, S. Z., Foster, M. J. & Boettcher, S. W. Accelerating water dissociation in bipolar membranes and for electrocatalysis. *Science* **369**, 1099–1103 (2020).
33. Larrazábal, G. O. Analysis of mass flows and membrane cross-over in CO_2 reduction at high current densities in an MEA-type electrolyzer. *ACS Appl. Mater. Interfaces* **11**, 41281–41228 (2019).
An analysis of how CO_2 moves throughout a reactor during CO_2 electrolysis, highlighting the importance of calculating the carbon mass balance, particularly when quantifying activity.
34. Ma, M. et al. Insights into the carbon balance for CO_2 electroreduction on Cu using gas diffusion electrode reactor designs. *Energy Environ. Sci.* **13**, 977–985 (2020).
35. Rabinowitz, J. A. & Kanan, M. W. The future of low-temperature carbon dioxide electrolysis depends on solving one basic problem. *Nat. Commun.* **11**, 5231 (2020).
An overview of how the formation of carbonate lowers the efficiency of many CO_2 reactor designs, highlighting the importance of new developments to advance the technology.
36. Dufek, E. J., Lister, T. E. & McIlwain, M. E. Bench-scale electrochemical system for generation of CO and syn-gas. *J. Appl. Electrochem.* **41**, 623–631 (2011).
37. Singh, M. R., Kwon, Y., Lum, Y., Ager, J. W. & Bell, A. T. Hydrolysis of electrolyte cations enhances the electrochemical reduction of CO_2 over Ag and Cu. *J. Am. Chem. Soc.* **138**, 13006–13012 (2016).
38. Gabardo, C. M. et al. Combined high alkalinity and pressurization enable efficient CO_2 electroreduction to CO. *Energy Environ. Sci.* **11**, 2531–2539 (2018).
39. Chen, C., Li, Y. & Yang, P. Address the 'alkalinity problem' in CO_2 electrolysis with catalyst design and translation. *Joule* **5**, 737–742 (2021).
40. Varela, A. S., Ju, W., Reier, T. & Strasser, P. Tuning the catalytic activity and selectivity of Cu for CO_2 electroreduction in the presence of halides. *ACS Catal.* **6**, 2136–2144 (2016).
41. McCrum, I. T., Akhade, S. A. & Janik, M. J. Electrochemical specific adsorption of halides on Cu 111, 100, and 211: a density functional theory study. *Electrochim. Acta* **173**, 302–309 (2015).
42. Gao, D., Scholten, F. & Roldan Cuenya, B. Improved CO_2 electroreduction performance on plasma-activated Cu catalysts via electrolyte design: halide effect. *ACS Catal.* **7**, 5112–5120 (2017).
43. Endrődi, B. et al. Multilayer electrolyzer stack converts carbon dioxide to gas products at high pressure with high efficiency. *ACS Energy Lett.* **4**, 1770–1777 (2019).
44. Jiang, K. et al. Isolated Ni single atoms in graphene nanosheets for high-performance CO_2 reduction. *Energy Environ. Sci.* **11**, 893–903 (2018).
45. Yin, Z. et al. An alkaline polymer electrolyte CO_2 electrolyzer operated with pure water. *Energy Environ. Sci.* **12**, 2455–2462 (2019).
46. Liu, Z. et al. Electrochemical generation of syngas from water and carbon dioxide at industrially important rates. *J. CO_2 Util.* **15**, 50–56 (2016).
47. Wang, Y. et al. Catalyst synthesis under CO_2 electroreduction favours faceting and promotes renewable fuels electrosynthesis. *Nat. Catal.* **3**, 98–106 (2020).
48. Li, F. et al. Molecular tuning of CO_2-to-ethylene conversion. *Nature* **577**, 509–513 (2020).
49. Salvatore, D. A. et al. Designing anion exchange membranes for CO_2 electrolysers. *Nat. Energy* **6**, 339–348 (2021).
50. Xia, C. et al. Continuous production of pure liquid fuel solutions via electrocatalytic CO_2 reduction using solid-electrolyte devices. *Nat. Energy* **4**, 776–785 (2019).
The use of a solid electrolyte device for the generation and isolation of formic acid, ethanol, acetic acid and n-propanol.
51. Yang, H., Kaczur, J. J., Sajjad, S. D. & Masel, R. I. Electrochemical conversion of CO_2 to formic acid utilizing Sustainion membranes. *J. CO_2 Util.* **20**, 208–217 (2017).
52. Ma, S., Luo, R., Moniri, S., Lan, Y. & Kenis, P. J. A. Efficient electrochemical flow system with improved anode for the conversion of CO_2 to CO. *J. Electrochem. Soc.* **161**, F1124–F1131 (2014).
53. Jhong, H.-R. M. et al. A nitrogen-doped carbon catalyst for electrochemical CO_2 conversion to CO with high selectivity and current density. *ChemSusChem* **10**, 1094–1099 (2017).
54. Lee, W. H. et al. Highly selective and scalable CO_2 to CO—electrolysis using coral-nanostructured Ag catalysts in zero-gap configuration. *Nano Energy* **76**, 105030 (2020).
55. Ma, S., Liu, J., Sasaki, K., Lyth, S. M. & Kenis, P. J. A. Carbon foam decorated with silver nanoparticles for electrochemical CO_2 conversion. *Energy Technol.* **5**, 861–863 (2017).
56. Ma, S. et al. Carbon nanotube containing Ag catalyst layers for efficient and selective reduction of carbon dioxide. *J. Mater. Chem. A* **4**, 8573–8578 (2016).
57. Kim, B. et al. Over a 15.9% solar-to-CO conversion from dilute CO_2 streams catalyzed by gold nanoclusters exhibiting a high CO_2 binding affinity. *ACS Energy Lett.* **5**, 749–757 (2020).
58. Zhang, T. et al. Nickel–nitrogen–carbon molecular catalysts for high rate CO_2 electro-reduction to CO: on the role of carbon substrate and reaction chemistry. *ACS Appl. Energy Mater.* **3**, 1617–1626 (2020).
59. Möller, T. et al. Efficient CO_2 to CO electrolysis on solid Ni–N–C catalysts at industrial current densities. *Energy Environ. Sci.* **12**, 640–647 (2019).
60. Yang, H. et al. Carbon dioxide electroreduction on single-atom nickel decorated carbon membranes with industry compatible current densities. *Nat. Commun.* **11**, 593 (2020).
61. Wang, M. et al. CO_2 electrochemical catalytic reduction with a highly active cobalt phthalocyanine. *Nat. Commun.* **10**, 3602 (2019).
62. Torbensen, K. et al. Iron porphyrin allows fast and selective electrocatalytic conversion of CO_2 to CO in a flow cell. *Chem. Eur. J.* **26**, 3034–3038 (2020).
63. Corral, D. et al. Advanced manufacturing for electrosynthesis of fuels and chemicals from CO_2. *Energy Environ. Sci.* **14**, 3064–3074 (2021).
The use of a Cu catalyst in the presence of nitrogen-doped carbon reduces the deoxygenation of HOCCH intermediates to achieve 52% selectivity for ethanol formation.
64. Li, Y. C. et al. Binding site diversity promotes CO_2 electroreduction to ethanol. *J. Am. Chem. Soc.* **141**, 8584–8591 (2019).
65. Zhong, M. et al. Accelerated discovery of CO_2 electrocatalysts using active machine learning. *Nature* **581**, 178–183 (2020).
66. She, X. et al. Tandem electrodes for carbon dioxide reduction into C^{2+} products at simultaneously high production efficiency and rate. *Cell Rep. Phys. Sci.* **1**, 100051 (2020).
67. Chen, C. et al. Cu–Ag tandem catalysts for high-rate CO_2 electrolysis toward multicarbons. *Joule* **4**, 1688–1699 (2020).
68. Karapinar, D., Creissen, C. E., Rivera de la Cruz, J. G., Schreiber, M. W. & Fontecave, M. electrochemical CO2 reduction to ethanol with copper-based catalysts. *ACS Energy Lett.* **6**, 694–706 (2021).
69. Wang, X. et al. Efficient electrically powered CO_2-to-ethanol via suppression of deoxygenation. *Nat. Energy* **5**, 478–486 (2020).
70. Luo, M. et al. Hydroxide promotes carbon dioxide electroreduction to ethanol on copper via tuning of adsorbed hydrogen. *Nat. Commun.* **10**, 5814 (2019).
71. Jouny, M. et al. Formation of carbon–nitrogen bonds in carbon monoxide electrolysis. *Nat. Chem.* **11**, 846–851 (2019).
72. Hoang, T. T. H., Ma, S., Gold, J. I., Kenis, P. J. A. & Gewirth, A. A. Nanoporous copper films by additive-controlled electrodeposition: CO_2 reduction catalysis. *ACS Catal.* **7**, 3313–3321 (2017).
73. Zhuang, T.-T. et al. Copper nanocavities confine intermediates for efficient electrosynthesis of C_3 alcohol fuels from carbon monoxide. *Nat. Catal.* **1**, 946–951 (2018).
74. Luc, W. et al. Two-dimensional copper nanosheets for electrochemical reduction of carbon monoxide to acetate. *Nat. Catal.* **2**, 423–430 (2019).
75. Ripatti, D. S., Veltman, T. R. & Kanan, M. W. Carbon monoxide gas diffusion electrolysis that produces concentrated C_2 products with high single-pass conversion. *Joule* **3**, 240–256 (2019).
76. Xia, R., Zhang, S., Ma, X. & Jiao, F. Surface-functionalized palladium catalysts for electrochemical CO_2 reduction. *J. Mater. Chem. A* https://doi.org/10.1039/D0TA03427D (2020).
77. Wang, V. C.-C., Islam, S. T. A., Can, M., Ragsdale, S. W. & Armstrong, F. A. Investigations by protein film electrochemistry of alternative reactions of nickel-containing carbon monoxide dehydrogenase. *J. Phys. Chem. B* **119**, 13690–13697 (2015).

78. Nwabara, U. O., Cofell, E. R., Verma, S., Negro, E. & Kenis, P. J. A. Durable cathodes and electrolyzers for the efficient aqueous electrochemical reduction of CO_2. *ChemSusChem* **13**, 855–875 (2020).
79. Hammer, B. & Norskov, J. K. Why gold is the noblest of all the metals. *Nature* **376**, 238–240 (1995).
80. Wilde, P. et al. Is Cu instability during the CO_2 reduction reaction governed by the applied potential or the local CO concentration? *Chem. Sci.* **12**, 4028–4033 (2021).
81. Martić, N. et al. $Ag_2Cu_2O_3$—a catalyst template material for selective electroreduction of CO to C_{2+} products. *Energy Environ. Sci.* **13**, 2993–3006 (2020).
82. Jovanov, Z. P., Ferreira de Araujo, J., Li, S. & Strasser, P. Catalyst preoxidation and EDTA electrolyte additive remedy activity and selectivity declines during electrochemical CO_2 reduction. *J. Phys. Chem. C.* **123**, 2165–2174 (2019).
83. Jeon, H. S., Kunze, S., Scholten, F. & Roldan Cuenya, B. Prism-shaped Cu nanocatalysts for electrochemical CO_2 reduction to ethylene. *ACS Catal.* **8**, 531–535 (2018).
84. Ganesan, S. et al. Impact of cationic Impurities on low-Pt loading PEFC Cathodes. *ECS Trans.* **66**, 19–27 (2015).
85. Chlistunoff, J., Davey, J. R., Rau, K. C., Mukundan, R. & Borup, R. L. PEMFC gas diffusion media degradation determined by acid–base titrations. *ECS Trans.* **50**, 521–529 (2013).
86. Xu, Y. et al. Self-cleaning CO_2 reduction systems: unsteady electrochemical forcing enables stability. *ACS Energy Lett.* **6**, 809–815 (2021).
87. Dufek, E. J., Lister, T. E., Stone, S. G. & McIlwain, M. E. Operation of a pressurized system for continuous reduction of CO_2. *J. Electrochem. Soc.* **159**, F514–F517 (2012).
88. Verma, S., Lu, X., Ma, S., Masel, R. I. & Kenis, P. J. A. The effect of electrolyte composition on the electroreduction of CO_2 to CO on Ag based gas diffusion electrodes. *Phys. Chem. Chem. Phys.* **18**, 7075–7084 (2016).
89. Edwards, J. P. et al. Efficient electrocatalytic conversion of carbon dioxide in a low-resistance pressurized alkaline electrolyzer. *Appl. Energy* **261**, 114305 (2020).
90. Li, H. & Oloman, C. Development of a continuous reactor for the electro-reduction of carbon dioxide to formate—part 2: scale-up. *J. Appl. Electrochem.* **37**, 1107–1117 (2007).
91. Whipple, D. T., Finke, E. C. & Kenis, P. J. A. Microfluidic reactor for the electrochemical reduction of carbon dioxide: the effect of pH. *Electrochem. Solid-State Lett.* **13**, B109 (2010).
92. Lu, X., Leung, D. Y. C., Wang, H. & Xuan, J. A high performance dual electrolyte microfluidic reactor for the utilization of CO_2. *Appl. Energy* **194**, 549–559 (2017).
93. Grigioni, I. et al. CO2 electroreduction to formate at a partial current density of 930 mA cm^{-2} with InP colloidal quantum dot derived catalysts. *ACS Energy Lett.* **6**, 79–84 (2021).
94. Cook, R. L. High rate gas phase CO_2 reduction to ethylene and methane using gas diffusion electrodes. *J. Electrochem. Soc.* **137**, 607 (1990).
95. Li, J. et al. Copper adparticle enabled selective electrosynthesis of *n*-propanol. *Nat. Commun.* **9**, 4614 (2018).
96. Pang, Y. et al. Efficient electrocatalytic conversion of carbon monoxide to propanol using fragmented copper. *Nat. Catal.* **2**, 251–258 (2019).
97. Wang, X. et al. Efficient upgrading of CO to C_3 fuel using asymmetric C–C coupling active sites. *Nat. Commun.* **10**, 5186 (2019).
98. Endrődi, B. et al. Operando cathode activation with alkali metal cations for high current density operation of water-fed zero-gap carbon dioxide electrolysers. *Nat. Energy* **6**, 439–448 (2021).
99. Jeanty, P. et al. Upscaling and continuous operation of electrochemical CO_2 to CO conversion in aqueous solutions on silver gas diffusion electrodes. *J. CO_2 Util.* **24**, 454–462 (2018).
100. Liu, Z., Yang, H., Kutz, R. & Masel, R. I. CO_2 electrolysis to CO and O_2 at high selectivity, stability and efficiency using Sustainion membranes. *J. Electrochem. Soc.* **165**, J3371–J3377 (2018).
101. Mohammadian, S. H., Aït-Kadi, D. & Routhier, F. Quantitative accelerated degradation testing: practical approaches. *Reliab. Eng. Syst. Saf.* **95**, 149–159 (2010).
102. Dutta, A. et al. Activation of bimetallic AgCu foam electrocatalysts for ethanol formation from CO_2 by selective Cu oxidation/reduction. *Nano Energy* **68**, 104331 (2020).
103. Wang, L. et al. Electrochemical carbon monoxide reduction on polycrystalline copper: effects of potential, pressure, and pH on selectivity toward multicarbon and oxygenated products. *ACS Catal.* **8**, 7445–7454 (2018).
104. Huang, J. E. et al. CO_2 electrolysis to multicarbon products in strong acid. *Science* **372**, 1074–1078 (2021).
105. Ma, M., Kim, S., Chorkendorff, I. & Seger, B. Role of ion-selective membranes in the carbon balance for CO_2 electroreduction via gas diffusion electrode reactor designs. *Chem. Sci.* **11**, 8854–8861 (2020).
106. Lu, X. et al. High-performance electrochemical CO_2 reduction cells based on non-noble metal catalysts. *ACS Energy Lett.* **3**, 2527–2532 (2018).
107. Chen, J. et al. Efficient electroreduction of CO_2 to CO by Ag-decorated S-doped g-C_3N_4/CNT nanocomposites at industrial scale current density. *Mater. Today Phys.* **12**, 100176 (2020).
108. Ye, K. et al. In situ reconstruction of a hierarchical Sn–Cu/SnO_x core/shell catalyst for high-performance CO_2 electroreduction. *Angew. Chem. Int. Ed.* **59**, 4814–4821 (2020).
109. Lai, Q., Yang, N. & Yuan, G. Highly efficient In–Sn alloy catalysts for electrochemical reduction of CO_2 to formate. *Electrochem. Commun.* **83**, 24–27 (2017).
110. Lim, J., Kang, P. W., Jeon, S. S. & Lee, H. Electrochemically deposited Sn catalysts with dense tips on a gas diffusion electrode for electrochemical CO_2 reduction. *J. Mater. Chem. A* **8**, 9032–9038 (2020).

Acknowledgements

D.W., S.L., D.C., J.W., A.S., S.A.J., M.F., E.H.S., T.F.J. and C.H. acknowledge financial support from TotalEnergies SE. D.C., J.F., A.C., E.D. and S.B. contributed under the auspices of the US Department of Energy by Lawrence Livermore National Laboratory under contract DE-AC52-07NA27344 within the LDRD program 19-SI-005 and CRADA TC02307, IM: LLNL-JRNL-818573. J.W. and E.H.S. acknowledge funding from the Natural Sciences and Engineering Research Council (NSERC) of Canada. D.W. acknowledges financial support from the Lindemann Trust Fellowship. S.L. was funded by the Corps des Ponts, des Eaux et des Forêts. J.W. acknowledges financial support from the Ontario Graduate Scholarship (OGS) program and the NSERC Postgraduate Scholarship—Doctoral (PGS-D) program. D.C. acknowledges financial support from the Stanford Graduate Fellowship (SGF) and GEM Fellowship at Stanford University and Lawrence Livermore National Laboratory, respectively.

Competing interests

D.W. and S.L. are, respectively, the chief technology officer (CTO) and chief executive officer (CEO) of Dioxycle, which develops low-temperature CO_2 electrolysers. A.S. and S.A.J. are full-time employees of TotalEnergies SE, which is sponsoring R&D programmes focused on the 'development of a viable low-temperature CO_2 electrocatalysis technology' at Collège de France, Lawrence Livermore National Laboratory, Stanford University and the University of Toronto.

Additional information

Correspondence should be addressed to Edward H. Sargent, Thomas F. Jaramillo or Christopher Hahn.

Peer review information *Nature Energy* thanks Angel Irabien, Haotian Wang and the other, anonymous, reviewer(s) for their contribution to the peer review of this work.